

Quark mean field model with density dependent couplings for finite nuclei

Y. H. Tan², H. Shen^{1,2,3}, P. Z. Ning^{1,2,3}

¹*CCAST(World Lab.), P.O.Box 8730, Beijing 100080, China*

²*Department of Physics, Nankai University, Tianjin 300071, China*

³*Institute of Theoretical Physics, Beijing 100080, China*

The quark mean field model, which describes the nucleon using the constituent quark model, is applied to investigate the properties of finite nuclei. The couplings of the scalar and vector mesons with quarks are made density dependent through direct coupling to the scalar field so as to reproduce the relativistic Brueckner-Hartree-Fock results of nuclear matter. The present model provides satisfactory results on the properties of spherical nuclei, and predicts an increasing size of the nucleon as well as a reduction of the nucleon mass in the nuclear environment.

PACS numbers: 12.39.-x, 21.65.+f, 24.10.Jv, 24.85.+p

I. INTRODUCTION

One of the most interesting topics in nuclear physics is to study the variations of hadron properties in nuclear medium. Experimentally, the EMC effect reveals the medium modification of the internal structure of the nucleon [1]. The EMC effect motivated many theoretical works on the study of hadrons in terms of quarks and gluons. At present, we are still far away to describe nucleons and nuclei in terms of quarks and gluons using quantum chromodynamics (QCD), which is believed to be the fundamental theory of strong interactions. Thus, it is desirable to build models which incorporate quark and gluon degrees of freedom and respect the established theories based on hadronic degrees of freedom. Such models are necessarily crude from various view points since the study of the nuclear many-body systems on the fundamental level is intractable.

The quark-meson coupling (QMC) model proposed by Guichon [2] provides a simple and attractive framework to incorporate quark degrees of freedom in the study of nuclear many-body systems. The model describes nuclear matter as nonoverlapping MIT bags in which the quarks interact self-consistently with structureless scalar and vector mesons in the mean field approximation. The QMC model has been subsequently extended with reasonable success to various problems of nuclear matter and finite nuclei [3–6]. The quark mean field (QMF) model as named in Ref. [7] took the constituent quark model for the nucleon instead of the MIT bag model, so that it could overcome the shortcoming of the QMC model as explained in Ref. [8]. The QMF model has been applied to study the properties of finite nuclei, where the coupling constants were determined by the saturation properties of nuclear matter [8].

In this paper, we introduce density dependent couplings for the QMF model, so that we can reproduce the relativistic Brueckner-Hartree-Fock (RBHF) results of nuclear matter [9]. The RBHF approach as a microscopic many-body theory based on hadronic degrees of freedom, provided very closely the nuclear matter saturation properties, where the coupling constants and the form factors of the one-boson exchange potential (OBEP) were fixed from the nucleon-nucleon scattering and the deuteron properties. The RBHF approach can be considered as parameter-free many-body theory, since all parameters in RBHF approach were adjusted to the two-nucleon problem at first. Encouraged by the success of the RBHF approach in describing nuclear matter properties, there were many applications of the RBHF results on finite nuclei [10–13]. The relativistic mean field (RMF) theory with density dependent couplings was developed for finite nuclei, as well as reproducing the RBHF results of nuclear matter. The RMF theory with density dependent couplings provided very good results on the nuclear properties as the binding energies and the nuclear radii with including the rearrangement contributions [11–13]. Both the RBHF and RMF approaches are based on hadronic degrees of freedom, where the nucleons and mesons are treated as structureless particles. Therefore, they are not applicable to study the quark effect in nuclei.

Hence, it is very interesting to connect the QMF model to the RBHF results by density dependent couplings, so that we can investigate the medium modification of the nucleon structure and finite nuclei properties, as well as reproducing the quantitative results of RBHF theory for nuclear matter simultaneously. The consideration to introduce density dependent couplings of mesons with quarks is based on the medium modifications of the meson properties. There are many works discussing the variations of hadron properties [14–17]. In the present model, the scalar mean field provides a strong attraction and as a consequence the constituent quark mass is reduced in nuclear medium. The mesons, which are actually composites of quarks, are influenced due to the presence of the scalar mean field. Therefore, the density dependent couplings modeled through direct coupling to the scalar field represents, in a way, self-interaction in the scalar field.

The paper is organized as follows. In Sec. II we describe the QMF model with density dependent couplings. In Sec. III we present the parameters used in this paper, and compare the nuclear matter results with RBHF results. We then apply this model to finite nuclei and discuss the variations of the nucleon properties inside nuclei in Sec. IV. Section V is devoted to the summary.

II. QUARK MEAN FIELD MODEL WITH DENSITY DEPENDENT COUPLING

In this section, we give a brief description of the QMF model with density dependent couplings. We follow the basic concept of the QMF model [7,8], in which the couplings of the mesons with quarks are constants. In the present work, we introduce density dependent couplings for the scalar (σ) and vector (ω) mesons with quarks, which are modeled as functions of the σ mean field. We include also the isovector meson, ρ , whose coupling with a quark is assume to be a constant for simplicity. We note that the contribution from the ρ meson is very weak for stable nuclei compared with those from the σ and ω mesons. In addition, the photon field should be included for finite system.

In the QMF model, the nucleon in nuclear medium is described in terms of the constituent quark model, in which the quarks couple with the σ , ω , and ρ mesons. We take the relativistic mean field (RMF) approximation [18–20] for the meson fields. In the constituent quark model, the quarks in a nucleon satisfy the following Dirac equation:

$$[i\gamma_\mu\partial^\mu - m_q + g_\sigma^q(\sigma)\sigma - g_\omega^q(\sigma)\omega\gamma^0 - g_\rho^q\rho\tau_3\gamma^0 - \chi_c] q(r) = 0. \quad (1)$$

where m_q is the constituent quark mass and χ_c the confinement. The $g_\sigma^q(\sigma)$ and $g_\omega^q(\sigma)$ as functions of the σ mean field, are the couplings of the σ and ω mesons with quarks, while the g_ρ^q denotes the coupling constant of the ρ meson with a quarks. We follow Ref. [7,8] to take into account the spin correlations and remove the spurious center of mass motion, and then work out the effective nucleon mass M_n^* .

For a static nuclear many-body system, the Lagrangian within the mean field approximation can be written as

$$\begin{aligned} \mathcal{L} = & \bar{\psi} [i\gamma_\mu\partial^\mu - M_n^*(\sigma) - g_\omega(\sigma)\omega\gamma^0 - g_\rho\rho\tau_3\gamma^0] \psi \\ & - \frac{1}{2} [(\nabla\sigma)^2 + m_\sigma^2\sigma^2] + \frac{1}{2} [(\nabla\omega)^2 + m_\omega^2\omega^2] + \frac{1}{2} [(\nabla\rho)^2 + m_\rho^2\rho^2] \\ & - \bar{\psi} \left[\frac{e}{2} (1 + \tau_3) \gamma^0 A \right] \psi + \frac{1}{2} (\nabla A)^2. \end{aligned} \quad (2)$$

Here, ψ denotes the nucleon fields; σ , ω , and ρ are the σ , ω , and ρ meson mean fields with masses m_σ , m_ω , and m_ρ , respectively; A denotes the photon field. The nuclear many-body system can be solved with the change of the nucleon properties under the influence of the scalar mean field, which is exclusively expressed in the effective nucleon mass, $M_n^*(\sigma)$, as a function of the σ mean field. The ω and ρ mean fields do not cause any change of the nucleon properties [21], and they appear merely as the energy shift. The relations between nucleon-meson couplings and quark-meson couplings have been given in Ref. [8] as $g_\omega(\sigma) = 3g_\omega^q(\sigma)$ and $g_\rho = g_\rho^q$. We will apply the present model to study the properties of nuclear matter and finite nuclei in the following two sections.

III. PARAMETERS AND NUCLEAR MATTER RESULTS

In this section we will show the numerical results of nuclear matter and discuss the density dependent couplings. The change of the nucleon properties under the influence of the σ mean field has been studied in Ref. [8], where the effective nucleon mass, M_n^* , has been shown as a function of the quark mass correction, δm_q . Here δm_q is related to σ mean field as $\delta m_q = g_\sigma^q(\sigma)\sigma$. We take the same quark mass and two types of confinement ($\chi_c = \frac{1}{2}kr^2$ and $\chi_c = \frac{1}{2}kr^2(1 + \gamma^0)/2$ with $k = 1000 \text{ MeV}/\text{fm}^2$) as those used in Ref. [8].

To perform the nuclear matter calculation, we take the Lagrangian given in Eq. (2), in which all the derivative terms of the meson fields vanish for infinite nuclear matter due to the translational invariance. Then, the nucleons and mesons obey the following Euler-Lagrange equations,

$$[i\gamma_\mu\partial^\mu - M_n^*(\sigma) - g_\omega(\sigma)\omega\gamma^0 - g_\rho\rho\tau_3\gamma^0]\psi = 0, \quad (3)$$

$$\begin{aligned} m_\sigma^2 \sigma &= -\frac{\partial M_n^*(\sigma)}{\partial\sigma} \langle \bar{\psi}\psi \rangle - \frac{\partial g_\omega(\sigma)}{\partial\sigma} \omega \langle \bar{\psi}\gamma^0\psi \rangle \\ &= -\frac{\partial M_n^*(\delta m_q)}{\partial\delta m_q} g_\sigma^q(\sigma) \langle \bar{\psi}\psi \rangle - \frac{\partial M_n^*(\delta m_q)}{\partial\delta m_q} \frac{\partial g_\sigma^q(\sigma)}{\partial\sigma} \sigma \langle \bar{\psi}\psi \rangle - 3 \frac{\partial g_\omega^q(\sigma)}{\partial\sigma} \omega \langle \bar{\psi}\gamma^0\psi \rangle, \end{aligned} \quad (4)$$

$$m_\omega^2 \omega = g_\omega(\sigma)\langle\bar{\psi}\gamma^0\psi\rangle = 3g_\omega^q(\sigma)\langle\bar{\psi}\gamma^0\psi\rangle, \quad (5)$$

$$m_\rho^2 \rho = g_\rho\langle\bar{\psi}\tau_3\gamma^0\psi\rangle = g_\rho^q\langle\bar{\psi}\tau_3\gamma^0\psi\rangle. \quad (6)$$

Here, the bracket $\langle \rangle$ means the expectation value of the operator between the nuclear ground state. We note that the appearance of the last two terms in Eq. (4) is due to the variable couplings, which is similar to the inclusion of the rearrangement terms in the density dependent RMF approach based on hadronic degrees of freedom [11]. The effective nucleon mass M_n^* and its derivative with respect to the δm_q has been studied in Ref. [8]. We take the meson masses as $m_\sigma = 550$ MeV, $m_\omega = 783$ MeV, and $m_\rho = 770$ MeV.

We introduce density dependent couplings, $g_\sigma^q(\sigma)$ and $g_\omega^q(\sigma)$, in the present model. This consideration is based on the variation of meson properties as the nuclear environment changes. The mesons, which are actually composites of quarks, are influenced by the σ mean field [16,17]. The quark-meson couplings in nuclear medium may be modified as density increases. It is therefore reasonable to attempt density dependent couplings, which contain the complicated medium modification effectively. This treatment is similar in spirit to the density dependent RMF approach based on hadronic degrees of freedom, which provided a realistic description of bulk properties of finite nuclei and nuclear matter [10–13]. The nucleon-meson couplings in the density dependent RMF approach were found to decrease with increasing nuclear matter density. This suggests a decreasing quark-meson couplings due to the relations between the nucleon-meson couplings with the quark-meson couplings.

we model the density dependent couplings, g_σ^q and g_ω^q , through direct couplings to the σ mean field. We parameterize these variable couplings as

$$g_\sigma^q(\sigma) = a_\sigma - b_\sigma\sigma^{1/3}, \quad (7)$$

$$g_\omega^q(\sigma) = a_\omega - b_\omega\sigma^{1/3}. \quad (8)$$

With these formulas, it is possible to reproduce the scalar and vector potentials of the RBHF theory for symmetric nuclear matter within a good accuracy. We list the parameters of a_i and b_i in Table I, which are determined by the RBHF results with potential A [9]. The parameter g_ρ^q , which is still a constant for simplicity, is taken as $g_\rho^q = 4$, so that we can get the symmetry energy to be around 35 MeV.

In Fig. 1, we plot the scalar and vector potentials, U_S and U_V , as functions of the nuclear matter density ρ . The RBHF results [9] are marked by solid dots, as well as the results in the RMF model with TM1 parameter set [20] by dotted curve for comparison. We show in Fig. 2 the energy per nucleon, E/A , as a function of density ρ . The solid and dashed curves, which are the results of the present model with two types of confinement, are almost identical. We note that the saturation density, binding energy and incompressibility of the solid curve in Fig. 2 are 0.16 fm^{-3} , -15.5 MeV and 159 MeV, respectively. We found there exist slight differences between the RBHF results and those in the present model in Fig. 2, which is partly due to the appearance of the rearrangement terms in Eq. (4). The importance of rearrangement terms in a relativistic density dependent field theory has been discussed extensively in Ref. [11].

IV. FINITE NUCLEI RESULTS

In this section we will present the calculated results of some spherical nuclei and discuss the variations of the nucleon properties inside nuclei. The meson mean fields in a spherically symmetric nucleus are functions of the radial coordinate r . Here, we follow the prescription of Ref. [5,8] and assume the nucleons obey the Dirac equation,

$$\left[i\gamma_\mu\partial^\mu - M_n^*(\sigma) - g_\omega(\sigma)\omega(r)\gamma^0 - g_\rho\rho(r)\tau_3\gamma^0 - \frac{e}{2}(1 + \tau_3)A(r)\gamma^0 \right] \psi = 0, \quad (9)$$

where the effective nucleon mass M_n^* is a function of the scalar mean field σ . The meson mean fields (σ , ω , ρ) and the photon field (A) satisfy the following Klein-Gordon equations,

$$\begin{aligned} \Delta\sigma(r) - m_\sigma^2\sigma(r) &= \frac{\partial M_n^*(\sigma)}{\partial\sigma}\langle\bar{\psi}\psi\rangle + \frac{\partial g_\omega(\sigma)}{\partial\sigma}\omega(r)\langle\bar{\psi}\gamma^0\psi\rangle \\ &= \frac{\partial M_n^*(\delta m_q)}{\partial\delta m_q}g_\sigma^q(\sigma)\langle\bar{\psi}\psi\rangle + \frac{\partial M_n^*(\delta m_q)}{\partial\delta m_q}\frac{\partial g_\sigma^q(\sigma)}{\partial\sigma}\sigma(r)\langle\bar{\psi}\psi\rangle + 3\frac{\partial g_\omega^q(\sigma)}{\partial\sigma}\omega(r)\langle\bar{\psi}\gamma^0\psi\rangle, \end{aligned} \quad (10)$$

$$\Delta\omega(r) - m_\omega^2\omega(r) = -g_\omega(\sigma)\langle\bar{\psi}\gamma^0\psi\rangle = -3g_\omega^q(\sigma)\langle\bar{\psi}\gamma^0\psi\rangle, \quad (11)$$

$$\Delta\rho(r) - m_\rho^2\rho(r) = -g_\rho\langle\bar{\psi}\tau_3\gamma^0\psi\rangle = -g_\rho^q\langle\bar{\psi}\tau_3\gamma^0\psi\rangle, \quad (12)$$

$$\Delta A(r) = -\frac{e}{2}\langle\bar{\psi}(1 + \tau_3)\gamma^0\psi\rangle. \quad (13)$$

We solve the above equations self-consistently using the parameters determined by the RBHF results of nuclear matter with potential A . In Fig. 3 and 4, we plot the charge density distributions for ^{40}Ca and ^{208}Pb , respectively. The experimental values taken from Ref. [23] are shown by solid curves. The calculated results with scalar confining potential ($\chi_c = \frac{1}{2}kr^2$) are shown by dashed curves, while those with scalar-vector confining potential ($\chi_c = \frac{1}{2}kr^2(1 + \gamma^0)/2$) by dash-dotted curves. The curves with two types of confinement are very close, since the parameters used here are determined by the same RBHF results. The theoretical central densities are slightly higher than the experimental values, which is related to the RBHF results used in determining the parameters. The dependence of the finite nuclei properties on the RBHF results were discussed in more detail in Refs. [10,12]. The calculated results in the present model for the binding energies per nucleon E/A , the rms charge radii R_c , and the spin-orbit splitting ΔE_{LS} are compared with the experimental values in Table II. The experimental data taken from Refs. [23,24] are listed in the last column. The results with two types of confinement agree very well with the experiment, and no explicit difference between them. In Table III and IV, the single particle energies of ^{40}Ca and ^{208}Pb are compared with the experimental data [24]. We show in Fig. 5 and 6 the scalar and vector mean fields (σ and ω) as functions of r for ^{40}Ca and ^{208}Pb . Here, the results with $\chi_c = \frac{1}{2}kr^2$ are given by solid curves, while those with $\chi_c = \frac{1}{2}kr^2(1 + \gamma^0)/2$ by dashed curves. Again, the corresponding results with two types of confinement are very similar due to the same reason as mentioned before.

It is very interesting to see the variations of the nucleon properties inside nuclei. We plot in Fig. 7 and 8 the ratios of the nucleon rms radius and effective mass in ^{40}Ca and ^{208}Pb to those in free space, R/R_0 and M_n^*/M_n , as functions of nuclear radial coordinate r . We find the model with $\chi_c = \frac{1}{2}kr^2(1 + \gamma^0)/2$ (dashed curves) gives near 10% increasing nucleon radius at the center of the nuclei, while that with $\chi_c = \frac{1}{2}kr^2$ gives around 5% increase. The nucleon radius decrease to its value in free space from center to outside, as the scalar mean field decreasing. As for the effective nucleon mass, both scalar and scalar-vector confinement cases give around 40% reduction at the center of the nuclei. The curves with two types of confinement are almost identical. It is due to the reproduction of the RBHF scalar potential.

V. CONCLUSION

We have developed the QMF model with density dependent couplings, so that we can investigate the variations of the nucleon structure and finite nuclei properties, as well as reproducing the RBHF results of nuclear matter simultaneously. We introduced the density dependence of the couplings of mesons with quarks through direct couplings to the σ field based on the capability of σ field in influencing hadron properties. We have used the constituent quark model for the nucleon, which naturally allows the direct coupling of σ, ω , and ρ mesons with quarks. With the parameters determined by the RBHF results of nuclear matter, we can perform the numerical calculations for finite nuclei.

We have found the QMF model with density dependent couplings gave very successful descriptions of spherical nuclei. By comparison with the density dependent RMF approach on hadronic level, we have reproduced the properties of finite nuclei with the same or even better agreement to the experimental data. The present model with scalar confinement has the capability to produced better results on the binding energies per nucleon compared with those in Ref. [8]. Very weak dependence on the type of the confinement was found in the results of nuclear properties, which is due to the reproduction of the RBHF scalar and vector potentials for nuclear matter.

We have also investigated the variations of the nucleon properties in spherical nuclei. The QMF model with density dependent couplings can provide a significantly swollen nucleon radius in nuclear environment. We found the model with $\chi_c = \frac{1}{2}kr^2(1 + \gamma^0)/2$ predicted near 10% increasing nucleon radius at the center of nuclei, while that with $\chi_c = \frac{1}{2}kr^2$ gave around 5% increase. At the same time, around 40% reduction of the nucleon mass at the center of nuclei were predicted.

ACKNOWLEDGMENTS

One of the authors (H.S.) would like to thank H. Toki for valuable discussions. This work was supported in part by the National Natural Science Foundation of China.

-
- [1] J. J. Aubert *et al.*, EMC Collaboration, Phys. Lett. **123B**, 275 (1983).
 - [2] P. A. M. Guichon, Phys. Lett. **200B**, 235 (1988).
 - [3] K. Saito and A. W. Thomas, Nucl. Phys. **A574**, 659 (1994).
 - [4] P. A. M. Guichon, K. Saito, E. Rodionov, and A. W. Thomas, Nucl. Phys. **A601** 349 (1996).
 - [5] H. Muller and B. K. Jennings, Nucl. Phys. **A640**, 55 (1998).
 - [6] P. Wang, R. K. Su, H. Q. Song, and L. L. Zhang, Nucl. Phys. **A653**, 166 (1999).
 - [7] H. Toki, U. Meyer, A. Faessler, and R. Brockmann, Phys. Rev. C **58**, 3749 (1998).
 - [8] H. Shen and H. Toki, Phys. Rev. C **61**, 045205 (2000).
 - [9] R. Brockmann and R. Machleidt, Phys. Rev. C **42**, 1965 (1990).
 - [10] R. Brockmann and H. Toki, Phys. Rev. Lett. **68**, 3408 (1992).
 - [11] C. Fuchs, H. Lenske, and H. H. Wolter, Phys. Rev. C **52**, 3043 (1995).
 - [12] F. Ineichen, M. K. Weigel, and D. Von-Eiff, Phys. Rev. C **53**, 2158 (1996).
 - [13] H. Shen, Y. Sugahara, and H. Toki, Phys. Rev. C **55**, 1211 (1997).
 - [14] G. E. Brown and M. Rho, Phys. Rev. Lett **66**, 2720 (1991).
 - [15] C. Song, G. E. Brown, D. -P. Min, and M. Rho, Phys. Rev. C **56**, 2244 (1997).
 - [16] K. Saito and A. W. Thomas, Phys. Rev. C **51**, 2757 (1995).
 - [17] K. Saito, K. Tsushima, and A. W. Thomas, Phys. Rev. C **55**, 2637 (1997).
 - [18] B. D. Serot and J. D. Walecka, Adv. Nucl. Phys. **16**, 1 (1986).
 - [19] Y. K. Gambhir, P. Ring, and A. Thimet, Ann. Phys. (N.Y.) **198**, 132 (1990).
 - [20] Y. Sugahara and H. Toki, Nucl. Phys. **A579**, 557 (1994).
 - [21] S. Fleck, W. Bentz, K. Shimizu, and K. Yazaki, Nucl. Phys. **A510**, 731 (1990).
 - [22] Y. Shibata and H. Tezuka, Z. Phys. C **62**, 533 (1994).
 - [23] H. de Vries, C. W. de Jager, and C. de Vries, At. Data Nucl. Data Tables **36**, 495 (1987).
 - [24] X. Campi and D. W. Sprung, Nucl. Phys. **A194**, 401 (1972).

TABLE I. Parameters needed to reproduce the RBHF results of nuclear matter with potential A in Ref. [9]

	QMF ($\chi_c = \frac{1}{2}kr^2$)	QMF ($\chi_c = \frac{1}{2}kr^2(1 + \gamma^0)/2$)
a_σ	6.415	7.328
$b_\sigma(\text{fm}^{1/3})$	5.852	6.016
a_ω	7.543	7.543
$b_\omega(\text{fm}^{1/3})$	6.470	6.470

 TABLE II. Binding energies per nucleon (E/A), rms charge radii (R_c), and spin-orbit splittings for neutrons (ΔE_n) and protons (ΔE_p) are compared with the experimental data [23,24]. The energies are in MeV, and the radii are in fm.

		QMF ($\chi_c = \frac{1}{2}kr^2$)	QMF ($\chi_c = \frac{1}{2}kr^2(1 + \gamma^0)/2$)	Expt.
^{40}Ca	E/A	8.65	8.62	8.55
	R_c	3.46	3.45	3.45
	$\Delta E_n(1d_{5/2} - 1d_{3/2})$	4.5	4.5	6.3
	$\Delta E_p(1d_{5/2} - 1d_{3/2})$	4.4	4.5	7.2
^{48}Ca	E/A	8.58	8.55	8.67
	R_c	3.49	3.48	3.45
	$\Delta E_n(1d_{5/2} - 1d_{3/2})$	3.8	3.8	3.6
	$\Delta E_p(1d_{5/2} - 1d_{3/2})$	3.9	3.9	4.3
^{90}Zr	E/A	8.50	8.49	8.71
	R_c	4.29	4.28	4.26
	$\Delta E_n(2p_{3/2} - 2p_{1/2})$	1.2	1.3	0.5
	$\Delta E_p(2p_{3/2} - 2p_{1/2})$	1.2	1.2	
^{208}Pb	E/A	7.62	7.62	7.87
	R_c	5.57	5.57	5.50
	$\Delta E_n(2f_{7/2} - 2f_{5/2})$	1.6	1.6	1.8
	$\Delta E_p(1g_{9/2} - 1g_{7/2})$	2.6	2.5	4.0

 TABLE III. Single particle energies of neutron (n) and proton (p) for ^{40}Ca . The experimental data are taken from Ref. [24]. All energies are in MeV.

Shell	QMF ($\chi_c = \frac{1}{2}kr^2$)		QMF ($\chi_c = \frac{1}{2}kr^2(1 + \gamma^0)/2$)		Expt.	
	n	p	n	p	n	p
$1s_{1/2}$	51.3	43.1	51.5	43.3	50.0	50±11
$1p_{3/2}$	36.2	28.4	36.3	28.5	30.0	34±6
$1p_{1/2}$	33.6	25.7	33.7	25.8	27.0	34±6
$1d_{5/2}$	21.4	14.0	21.5	14.0	21.9	15.5
$1d_{3/2}$	16.9	9.5	17.0	9.6	15.6	8.3
$2s_{1/2}$	17.3	10.0	17.3	10.0	18.2	10.9

TABLE IV. Single particle energies of neutron (n) and proton (p) for ^{208}Pb . The experimental data are taken from Ref. [24]. All energies are in MeV.

Shell	QMF ($\chi_c = \frac{1}{2}kr^2$)		QMF ($\chi_c = \frac{1}{2}kr^2(1 + \gamma^0)/2$)		Expt.	
	n	p	n	p	n	p
$1s_{1/2}$	56.3	43.4	56.1	43.4		
$1p_{3/2}$	50.2	38.0	50.1	37.9		
$1p_{1/2}$	49.9	37.6	49.8	37.5		
$1d_{5/2}$	43.1	31.3	43.0	31.3		
$1d_{3/2}$	42.3	30.4	42.2	30.3		
$2s_{1/2}$	39.7	27.3	39.7	27.3		
$1f_{7/2}$	35.2	23.7	35.1	23.7		
$1f_{5/2}$	33.6	22.1	33.6	22.1		
$2p_{3/2}$	30.2	18.2	30.2	18.2		
$2p_{1/2}$	29.6	17.5	29.6	17.5		
$1g_{9/2}$	26.6	15.5	26.6	15.5		15.4
$1g_{7/2}$	24.2	13.0	24.2	13.0		11.4
$2d_{5/2}$	20.9	9.1	20.9	9.2		9.7
$2d_{3/2}$	19.7	7.9	19.7	8.0		8.4
$3s_{1/2}$	18.9	6.8	18.9	6.9		8.0
$1h_{11/2}$	17.8	6.9	17.8	7.0		9.4
$1h_{9/2}$	14.4		14.4		10.8	
$2f_{7/2}$	11.9		11.9		9.7	
$2f_{5/2}$	10.3		10.3		7.9	
$3p_{3/2}$	9.6		9.6		8.3	
$3p_{1/2}$	9.0		8.9		7.4	
$1i_{13/2}$	8.9		8.9		9.0	

FIGURE CAPTIONS

- Figure 1:** The scalar and vector potentials of nuclear matter, U_S and U_V , as functions of the nuclear matter density ρ . The results of the present model with $\chi_c = \frac{1}{2}kr^2$ are shown by solid curves, while those with $\chi_c = \frac{1}{2}kr^2(1+\gamma^0)/2$ are shown by dashed curves. The RBHF results with potential A in Ref. [9] are marked by solid dots, and the results in the RMF(TM1) model [20] are plotted by dotted curves for comparison.
- Figure 2:** The energy per nucleon, E/A , as functions of the nuclear matter density ρ . The curves are labeled as in Fig. 1.
- Figure 3:** The charge density distributions for ^{40}Ca compared with the experimental data (solid curve) [23]. The dash-dotted and dashed curves are the results in the present model with $\chi_c = \frac{1}{2}kr^2$ and $\chi_c = \frac{1}{2}kr^2(1+\gamma^0)/2$, respectively.
- Figure 4:** Same as Fig. 3 but for ^{208}Pb .
- Figure 5:** The scalar and vector mean fields, σ and ω , as functions of the radial coordinate r for ^{40}Ca . The results in the present model with $\chi_c = \frac{1}{2}kr^2$ are shown by solid curves, while those with $\chi_c = \frac{1}{2}kr^2(1+\gamma^0)/2$ are shown by dashed curves.
- Figure 6:** Same as Fig. 5 but for ^{208}Pb .
- Figure 7:** The ratios of the nucleon rms radius and effective mass in ^{40}Ca to those in free space, R/R_0 and M_n^*/M_n , as functions of the radial coordinate r . The results in the present model with $\chi_c = \frac{1}{2}kr^2$ are shown by solid curves, while those with $\chi_c = \frac{1}{2}kr^2(1+\gamma^0)/2$ are shown by dashed curves.
- Figure 8:** Same as Fig. 7 but for ^{208}Pb .

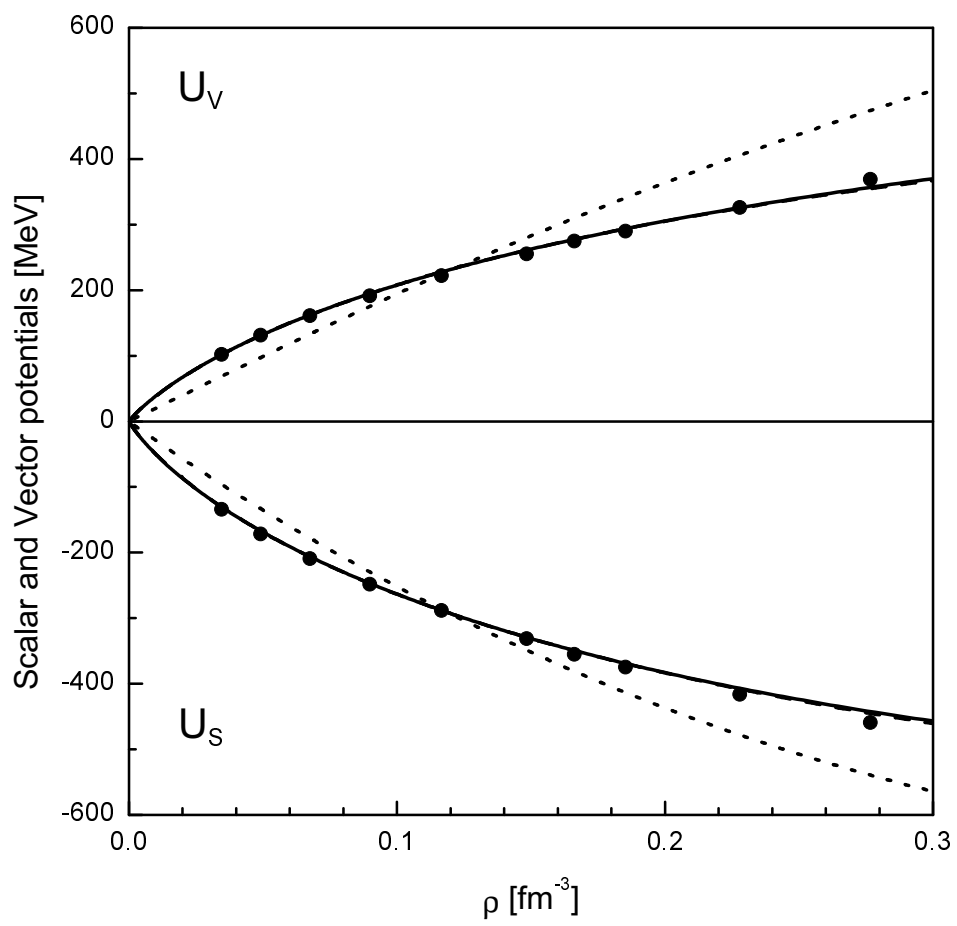


Fig. 1

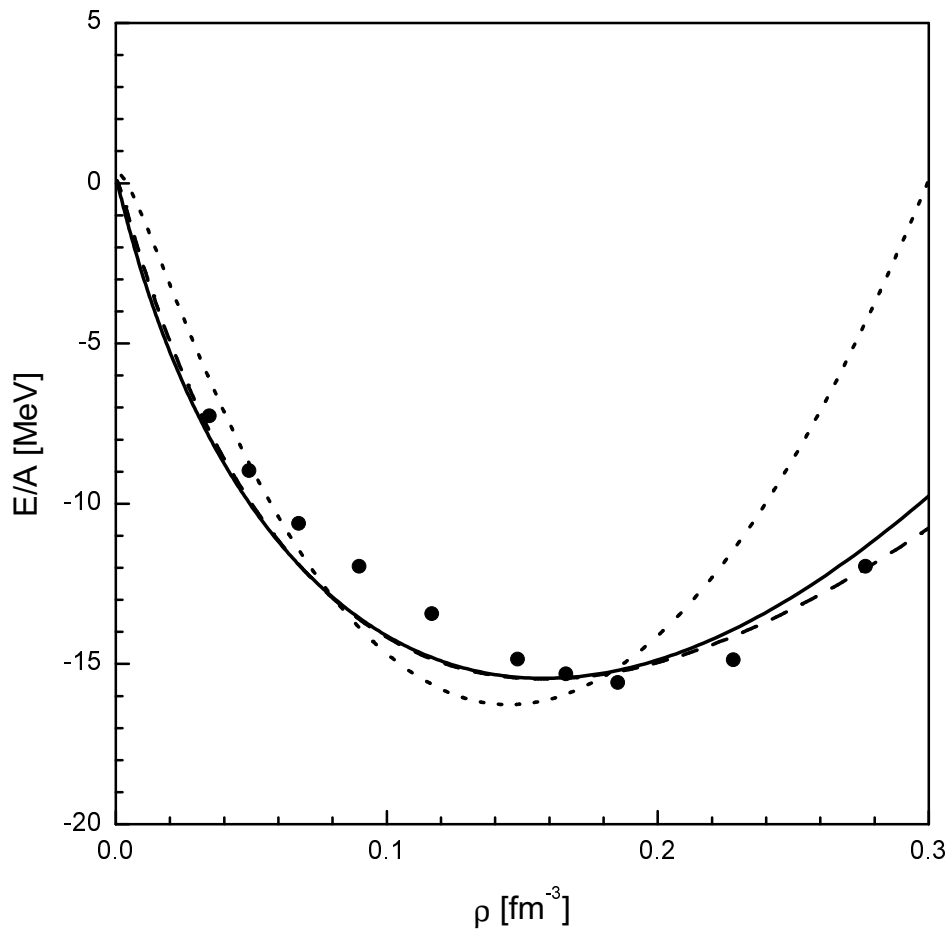


Fig. 2

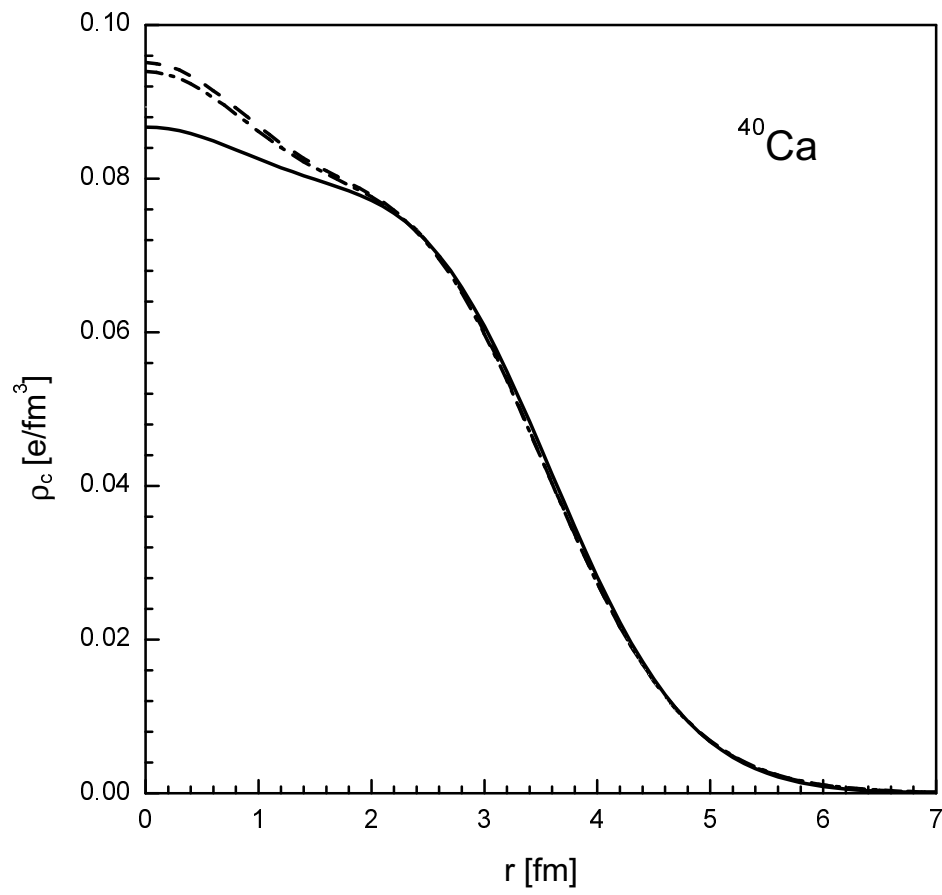


Fig. 3

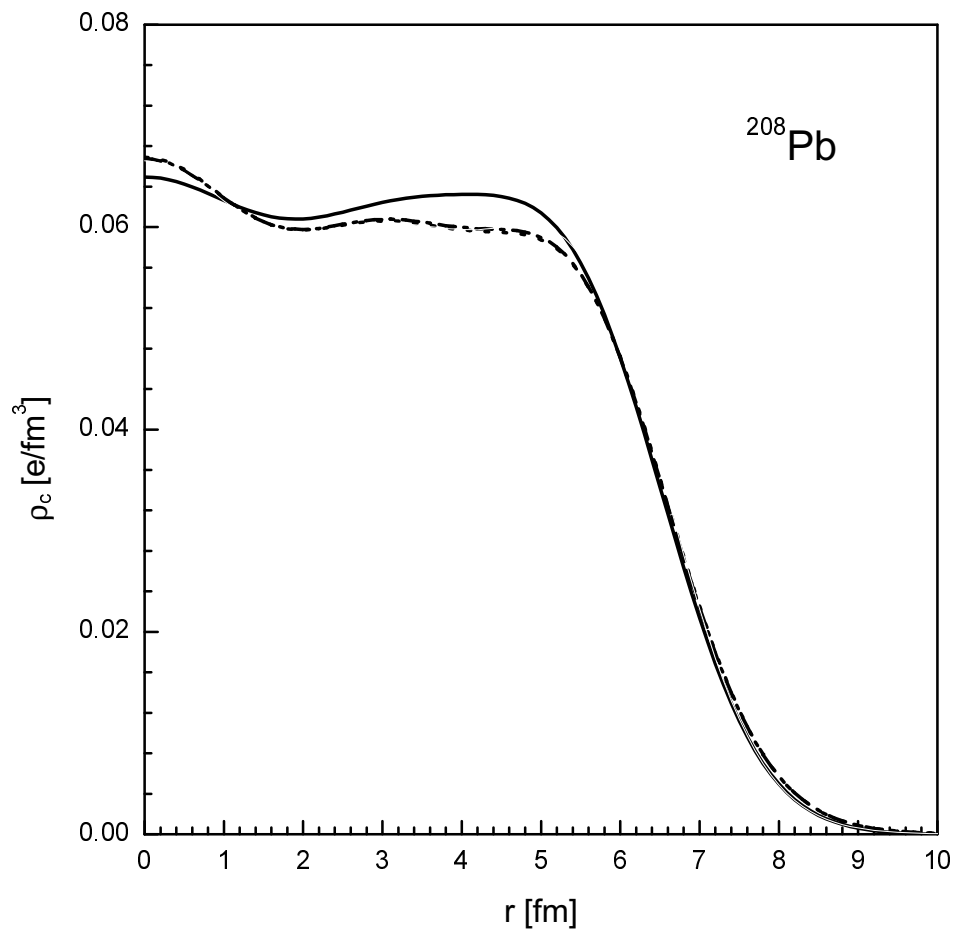


Fig. 4

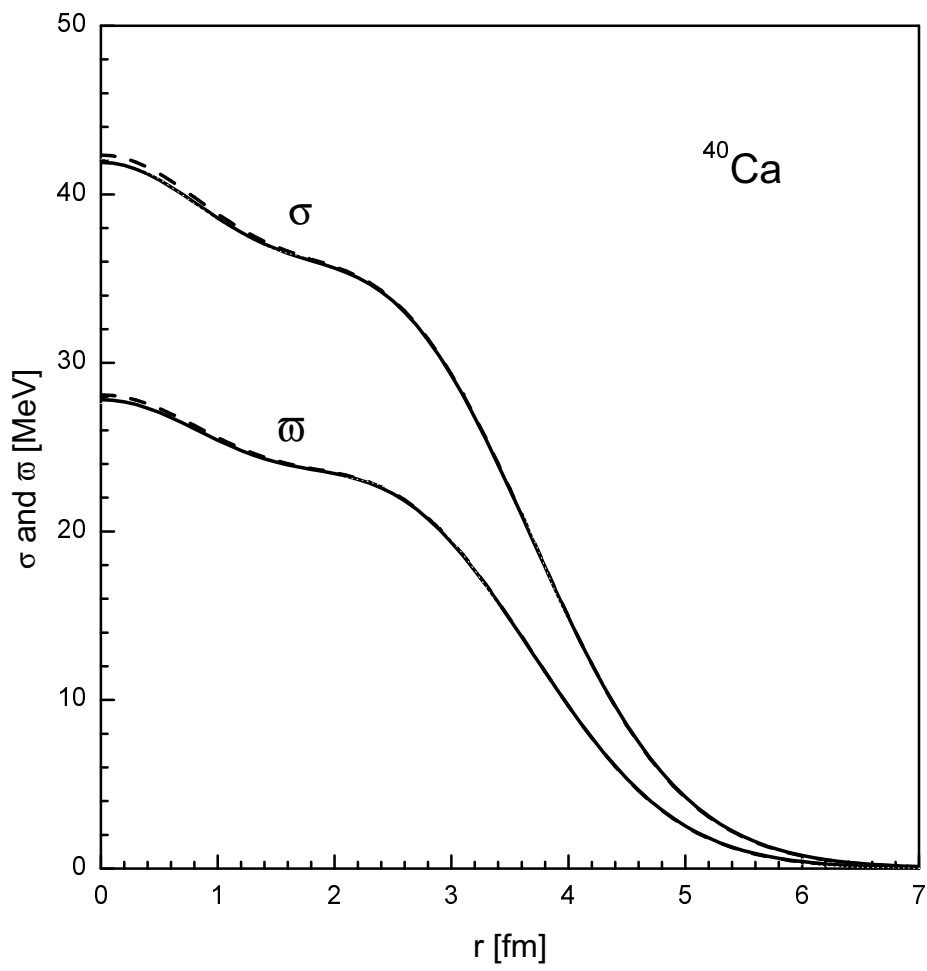


Fig. 5

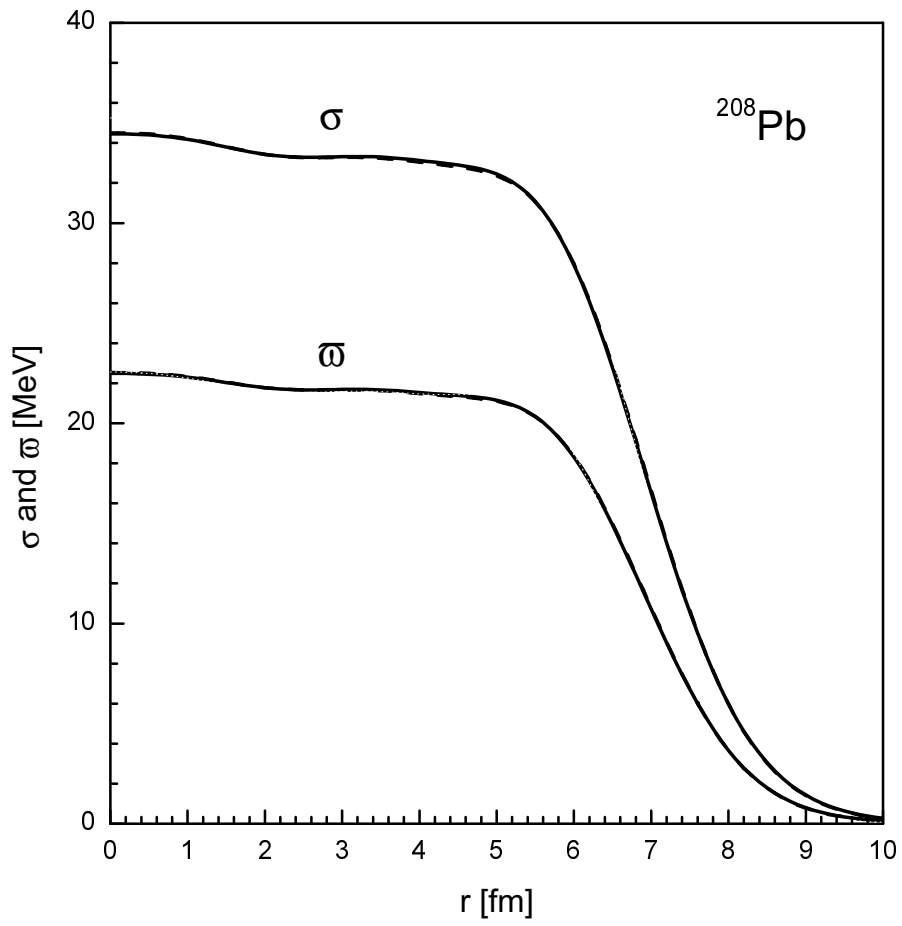


Fig. 6

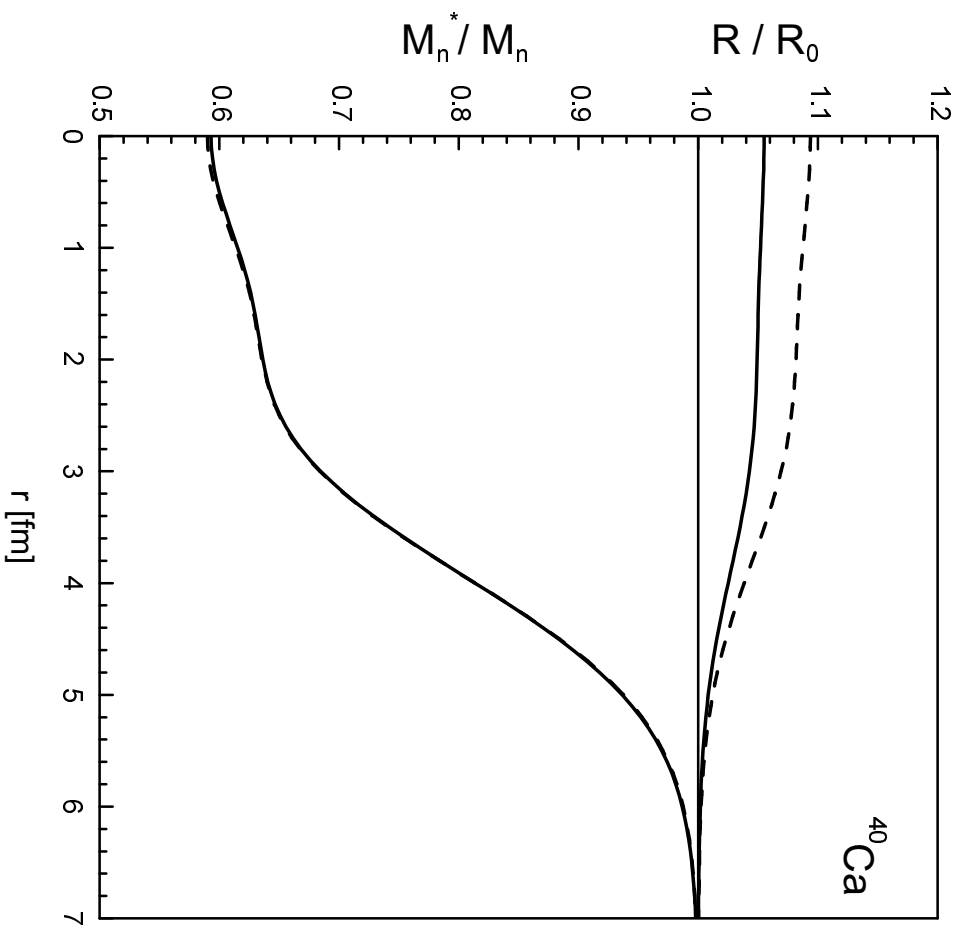


Fig. 7

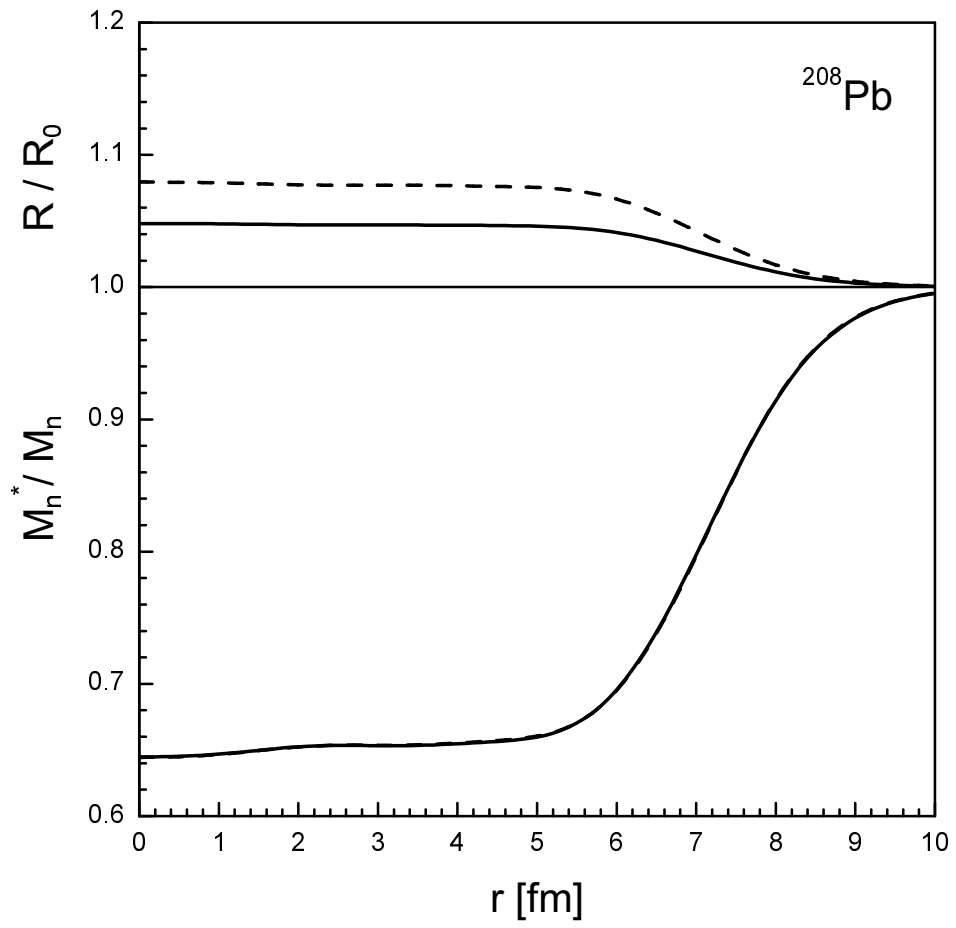


Fig. 8